Thermoelectric effects in silicene nanoribbons

K. Zberecki,[1] M. Wierzbicki,[1] J. Barnaś,[2] and R. Swirkowicz[1]
[1]*Faculty of Physics, Warsaw University of Technology, ul. Koszykowa 75, 00-662 Warsaw, Poland*
[2]*Faculty of Physics, Adam Mickiewicz University, ul. Umultowska 85, 61-614 Poznań, Poland and Institute of Molecular Physics, Polish Academy of Sciences, Smoluchowskiego 17, 60-179 Poznań, Poland*
(Received 14 May 2013; revised manuscript received 11 August 2013; published 3 September 2013)

Transport and thermoelectric coefficients (including also spin thermopower) of silicene nanoribbons with zigzag edges are investigated by *ab initio* numerical methods. Local spin density of such nanoribbons reveals edge magnetism. As in graphene, one finds antiferromagnetic and ferromagnetic ordering, with spin polarization at one edge antiparallel or parallel to that at the other edge, respectively. Thermoelectric properties, especially the Seebeck coefficient, significantly depend on the electronic band structure and are enhanced when the Fermi level is in the energy gap. However, the thermoelectric efficiency is significantly reduced when the phonon contribution to the heat conductance is included. This phonon contribution has been calculated numerically by two different methods. Transition from antiferromagnetic to ferromagnetic states leads to a large magnetoresistance as well as to a considerable magnetothermopower. Thermoelectric parameters in the antiparallel configuration, when spin polarization in the left part of the nanoribbon is opposite to that in the right part, are also analyzed.

DOI: 10.1103/PhysRevB.88.115404 PACS number(s): 73.63.−b, 75.75.−c

I. INTRODUCTION

There is currently an increasing interest in two-dimensional conducting materials such as graphene, a two-dimensional hexagonal lattice of carbon atoms. Graphene exhibits unusual transport properties which follow from its peculiar electronic structure. More specifically, the low-energy electronic states around the Fermi level (K points of the Brillouin zone) are described by the Dirac model and the electrons behave like massless particles. Owing to its promising electronic properties, such as high electron mobility and long spin diffusion length, graphene is considered as an ideal material for future nanoelectronic and spintronic devices.[1] Therefore, not only transport, but also magnetic and thermoelectric properties of graphene, are currently of great interest. Some possible applications of this novel material have been already proposed.[2,3]

Very recently, another two-dimensional material, silicene, has been fabricated.[4–7] Silicene is a two-dimensional hexagonal lattice of silicon atoms, but contrary to graphene, silicene has a buckled atomic structure: the two triangular sublattices are slightly displaced vertically. Electronic structure of the two-dimensional silicene is similar to that of graphene, i.e., silicene is a semimetal with low-energy states at the Fermi level described by the Dirac model. Spin-orbit interaction opens an energy gap at the Fermi level, but this gap, like in graphene, is rather small. The buckled atomic structure, however, gives rise to additional intrinsic spin-orbit interaction of Rashba form, which is absent in graphene, and which plays a significant role in spin transport.[8–10] Moreover, electric field normal to the atomic plane (gate voltage) can open an energy gap in silicene, but not in graphene.

From the application point of view, however, semiconducting transport properties are more desired than metallic or semimetallic ones. Thus, opening a gap at the Fermi level (K points) in the electronic spectrum is one of the key challenges. One way to achieve this objective is to form quasi-one-dimensional nanoribbons. Indeed, graphene nanoribbons (GNRs) were extensively studied in the past decade. In turn, fabrication of silicene nanoribbons (SiNRs) has been reported very recently,[5,6] which opened new perspectives for this novel material.[7,11]

Both graphene and silicene zigzag nanoribbons reveal edge magnetism, and in both cases antiferromagnetic (AFM) ordering of the edge magnetic moments (with spin polarization at one edge opposite to that at the other edge) corresponds to the lowest energy.[11,12] Electronic, mechanical, and magnetic properties of SiNRs have been studied recently by first-principles numerical methods.[11,13–15] In particular, electronic transport properties of SiNRs with zigzag edges (zSiNRs) have revealed a magnetoresistance effect[13] associated with transition of the edge magnetism from ferromagnetic (FM) to antiferromagnetic ordering. In turn, the giant magnetoresistance effect can be observed in narrow ribbons connected to ferromagnetic electrodes, when magnetizations of the electrodes change from antiparallel to parallel alignment, for instance in an external magnetic field.[14] Similar effects also occur in GNRs. For instance, a large magnetoresistance (close to 100% at low temperatures) associated with transition of the edge magnetic magnetic moments from AFM to FM configuration was found in GNRs.[16,17] Some preliminary calculations of thermoelectric properties of armchair as well as zigzag SiNRs have also been reported,[15] and relatively high thermopower S and some enhancement of the thermoelectric efficiency have been found at high temperatures for nonmagnetic armchair ribbons of some specific widths. Results obtained for zSiNRs have revealed less remarkable effects.

Thermoelectric properties of nanoscopic systems are currently of great interest due to the possibility of heat to electrical energy conversion at nanoscale, which is important for applications. Quantum confinement and transport blockade can lead to a considerable enhancement of the thermoelectric efficiency in such structures.[18–21] An interplay between the spin effects and thermoelectric properties in magnetic tunnel junctions and nanoscale systems has been also intensively studied in view of possible applications in spintronic devices.[22–25] As a result,

some new spin-related thermoelectric phenomena have been discovered. Certainly, the most spectacular spin-related effect is the spin thermopower (spin Seebeck effect), which is a spin analog of the usual electrical thermopower (Seebeck effect).[24] As the conventional thermopower consists in generation of electrical voltage in an open system by a temperature gradient, the spin thermopower corresponds to the thermal generation of spin voltage.

In this paper, we analyze thermoelectric properties of SiNRs with zigzag edges. The calculations have been carried out by *ab initio* numerical methods. Narrow Si nanoribbons, similarly to graphene ones,[26–28] reveal AFM ordering. Moreover, the corresponding electronic spectrum reveals an energy gap in the close vicinity of the Dirac points.[15,29] The AFM ordering is shown to have a strong influence on the transport properties, especially on the thermopower S, which can be considerably enhanced in zSiNRs with energy gaps. Thus, accurate determination of the gap width is crucial for the proper description of electronic transport and thermoelectric properties.

By applying an external magnetic field, one can switch the magnetic configuration in zSiNRs from an AFM to FM one. This change, in turn, leads to a large magnetoresistance effect. As we show in this paper, the thermopower also strongly depends on the magnetic configuration, so a considerable magnetothermopower can be observed. The latter effect is much stronger than in standard magnetic tunnel junctions.[22,23] Therefore, Si nanoribbons could be considered as interesting systems for applications in future nanoelectronics. A remarkably different Seebeck coefficients for various magnetic configurations were also found in zGNRs, which led to a large magneto Seebeck ratio.[30] Additionally, it was shown that the thermoelectric efficiency (figure of merit) is remarkably affected by the presence of energy gaps in the corresponding electronic spectra of zGNRs.[30] Furthermore, it was also shown that the spin Seebeck effect can occur in zGNRs with ferromagnetic ordering of the edge magnetic moments.[31]

The paper is organized as follows. In Sec. II, we describe the computational method used to determine transmission through the system. This transmission is subsequently used to determine the thermoelectric coefficients. The obtained numerical results on electronic transport and on electronic contribution to the heat transport in the limit of spin channel mixing are presented and discussed in Sec. III. In turn, spin thermoelectric properties are considered in Sec. IV. Heat transport mediated by phonons is presented and discussed in Sec. V. Summary and concluding remarks are presented in Sec. VI.

II. COMPUTATIONAL DETAILS: SPIN DENSITY AND TRANSMISSION FUNCTION

Electronic transport through zSiNRs was investigated numerically by *ab initio* calculations within the density functional theory (DFT) SIESTA code.[32] The spin-resolved energy-dependent transmission $T_\sigma(E)$ through zSiNRs of different widths was determined in terms of the nonequilibrium Green's function method (NGF) as implemented in the TRANSIESTA code.[33] As in Ref. 34, width of a zSiNR is characterized by the corresponding number N of zigzag chains in the ribbon. The nanoribbon edges were terminated with hydrogen atoms to remove the dangling bonds. The structures were

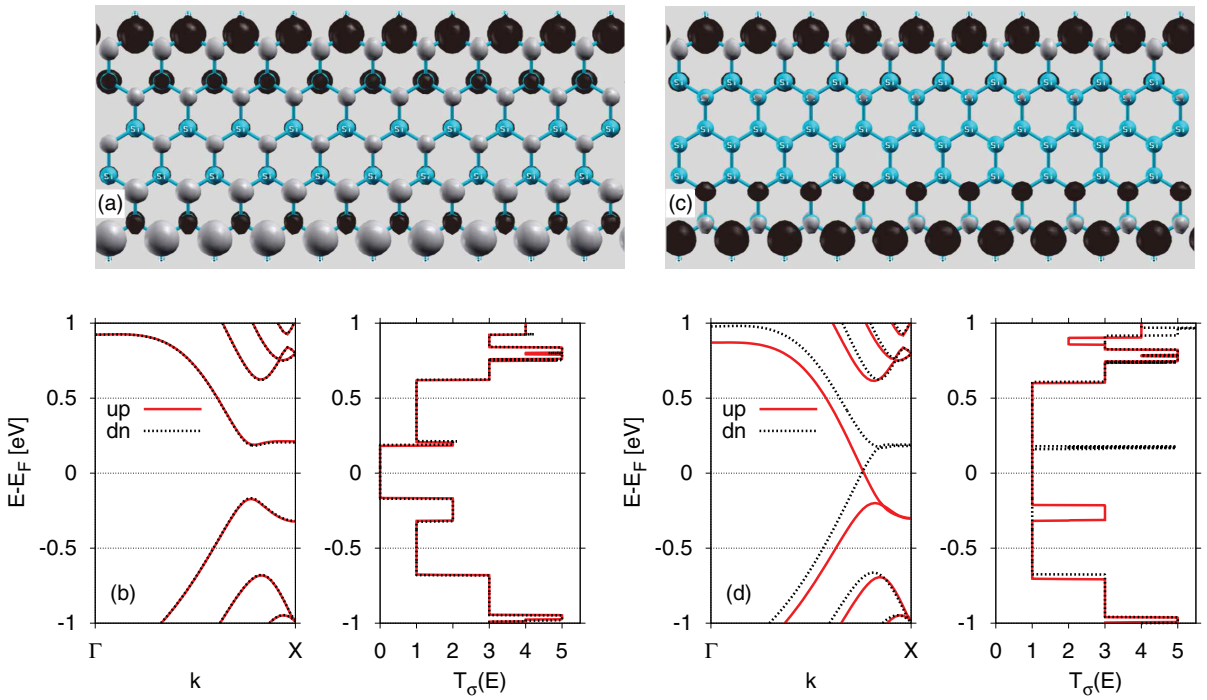

FIG. 1. (Color online) Spin density in the AFM (a) and FM (c) states, calculated within GGA approximation for zSiNRs with $N = 5$. The corresponding spin-resolved band structure and transmission function are shown in (b) and (d) for the AFM and FM configurations, respectively (up and dn stand for spin up and spin down, respectively). The energy is measured with respect to the corresponding Fermi energy E_F of an undoped structure (note E_F for AFM and FM states are generally different).

optimized until atomic forces converge to 0.02 eV/A. The atomic double-ζ polarized basis (DZP) was used and the grid mesh cutoff was set equal to 200 Ry. The generalized gradient approximation (GGA) with Perdew-Burke-Ernzerhof parametrization was applied for exchange-correlation part of the total energy functional.[35] For comparison, some calculations have been also performed within the local density approximation (LDA) with Ceperley-Alder parametrization (equivalent to the Perdew-Zunger one).[36,37] The performed calculations, similarly to those presented in Refs. 15 and 29, show that the AFM ordering is the most stable configuration in narrow zSiNRs. Spin configuration in both AFM and FM states is shown in Figs. 1(a) and 1(c), respectively. The energy difference between the FM and AFM configurations is rather small and for $N = 5$ it is equal to 0.02 eV. Thus, the configuration can be easily changed from the AFM to FM one by applying an external magnetic field. Therefore, the following calculations have been performed for both AFM and FM magnetic states.

Spin-polarized band structure and the corresponding spin-dependent transmission functions $T_\sigma(E)$ are presented in Figs. 1(b) and 1(d) for the AFM and FM configurations, respectively. Both band structure and transmission functions are significantly different in the two magnetic states. In the AFM case, the bands are spin degenerate, and an energy gap exists in the vicinity of $E = 0$ (corresponding to the Fermi level of an undoped system). Numerical calculations clearly show that the gap width decreases with increasing N. On the other hand, the transmission function for the FM configuration is spin dependent and is constant and finite in the vicinity of $E = 0$ for both spin orientations (indicating absence of energy gap) in agreement with Refs. 13 and 29. These results are also qualitatively similar to those obtained for graphene nanoribbons.[28]

III. THERMOELECTRIC PROPERTIES

In this section, we present numerical results on conventional thermoelectric properties of zSiNRs for $N = 5$, 6, and 7. By conventional thermoelectricity we mean here the effects that occur when the two spin channels are mixed in the contacts, so no spin thermopower can be observed. Later on, we will come back to the problem of spin thermoelectric phenomena.

In the linear response regime, the electric I and heat I_Q currents flowing through the system from left to right, when the electric potential and temperature of the left electrode are higher by ΔV and ΔT, respectively, can be written in the matrix form as[38]

$$\begin{pmatrix} I \\ I_Q \end{pmatrix} = \begin{pmatrix} e^2 L_0 & \frac{e}{T} L_1 \\ e L_1 & \frac{1}{T} L_2 \end{pmatrix} \begin{pmatrix} \Delta V \\ \Delta T \end{pmatrix}, \tag{1}$$

where e is the electron charge, while L_n $(n = 0,1,2)$ are defined as $L_n = -\frac{1}{h} \int dE\, T(E)(E-\mu)^n \frac{\partial f}{\partial E}$, with $f(E)$ being the equilibrium Fermi-Dirac distribution function corresponding to the chemical potential μ and temperature T (equal in both electrodes), and $T(E) = \sum_\sigma T_\sigma(E)$ denoting the total transmission through the system (maximum transmission is equal to the number of different quantum channels). We have determined the transmission function $T(E)$ using the *ab initio* method, as described in the preceding section. Having found $T(E)$, one can calculate the functions L_n by integrating over energy. Then, the electrical conductance G is given by $G = e^2 L_0$, while the electronic contribution to the thermal conductance κ_e is

$$\kappa_e = \frac{1}{T}\left(L_2 - \frac{L_1^2}{L_0}\right). \tag{2}$$

In turn, the thermopower $S = -\Delta V/\Delta T$ can be calculated from the formula[38]

$$S = -\frac{L_1}{|e| T L_0}. \tag{3}$$

Now, we consider the thermoelectric effects for some specific spin arrangements at the nanoribbon edges.

A. AFM configuration

The AFM configuration is the most stable configuration, at least in the regime of low temperatures. Later we will consider other configurations, which correspond to a higher total energy. Results obtained for the thermopower S and thermal conductance κ_e in the AFM state are shown in Fig. 2, where S and κ_e are presented as a function of the chemical potential μ. In reality, the chemical potential μ can be changed in the vicinity of the Fermi level of undoped system (corresponding to $\mu = 0$) either by p-type or n-type doping, which results in $\mu < 0$ and $\mu > 0$, respectively. In general, the chemical potential could be also varied with an external gate voltage.

Figure 1(b) clearly shows the presence of a relatively wide energy gap in the transmission function for the AFM configuration, which extends roughly from -0.2 to $+0.2$ eV. This gap has a strong influence on the transport and thermoelectric properties. First, the zero-temperature electrical conductance vanishes for chemical potential in the gap. As the temperature is sufficiently high, transport is mediated by activated electrons and/or holes. Consider the thermopower shown in Fig. 2(a). The thermopower vanishes at a certain point very close to $\mu = 0$ since the currents *via* electrons and holes (although both very small) compensate each other. When μ is positive (but still inside the gap), the thermopower is negative and achieves relatively large absolute values. The maximum of the absolute value of S appears when μ is at the distance of an order of several kT from the upper edge of the gap. The hole current is then blocked and the charge current is mediated by electrons. The thermocurrent flows then from right to left (electrons flow from left to right) and a positive voltage is needed to block the current. According to the definition, the thermopower is then negative. When, in turn, the chemical potential is negative (and still inside the gap), the thermocurrent is dominated by holes and flows from left to right. To block the current, one needs a negative voltage and therefore the thermopower is positive. Apart from the high peaks inside the gap, the thermopower is rather small in the remaining part of the considered range of μ. This is due to partial (or total) compensation of the contributions to thermocurrent from electrons and holes. When μ is already in the conduction band and slightly above the narrow peak in the transmission seen in Fig. 1(b), the thermopower becomes positive. For higher values of μ, it becomes negative again.

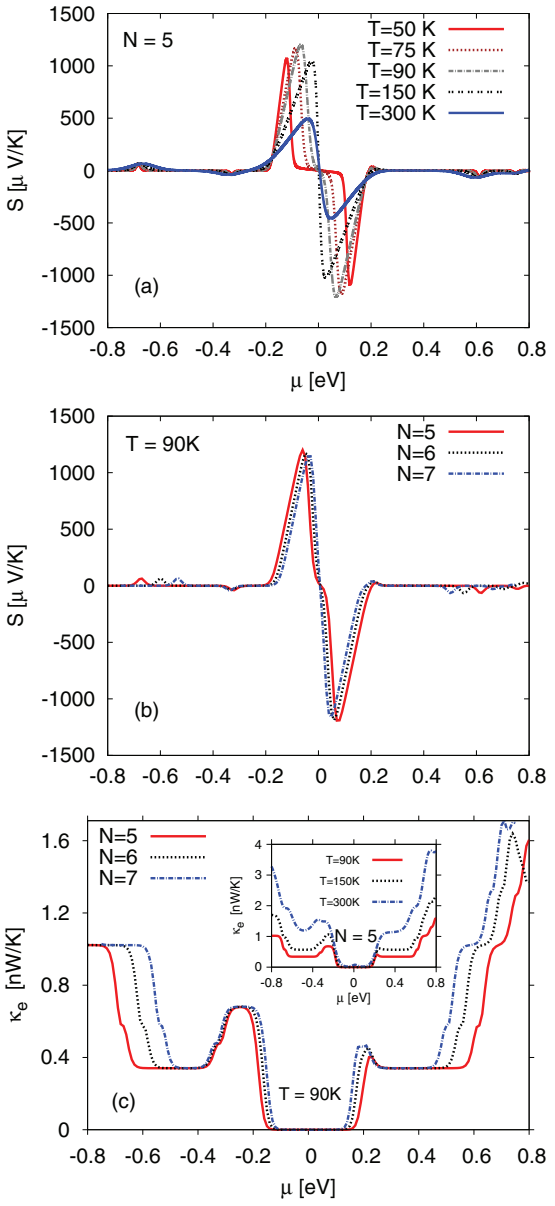

FIG. 2. (Color online) Thermopower S [(a) and (b)] and electronic thermal conductance κ_e (c) of zSiNRs in the AFM configuration as a function of the chemical potential μ, calculated within the GGA approximation for different values of N and temperature, as indicated.

Generally, the sign of thermopower depends on the details of electronic spectrum.

The thermopower strongly depends on temperature. With increasing T, the intensities of the main peaks are considerably reduced, although S is enhanced in a narrow region of $|\mu|$ around $\mu = 0$ [see Fig. 2(a)]. Thus, quite remarkable values of S can be achieved at high temperatures for very small n- or p-type doping, despite the energy gap in the transmission. Similar behavior of the thermopower S can be observed also in the nanoribbons with $N = 6$ and 7 [see Fig. 2(b)]. Some small differences follow from a decrease in the energy gap width for wider nanoribbons.

To understand the temperature dependence of the thermopower, especially when the chemical potential is in the

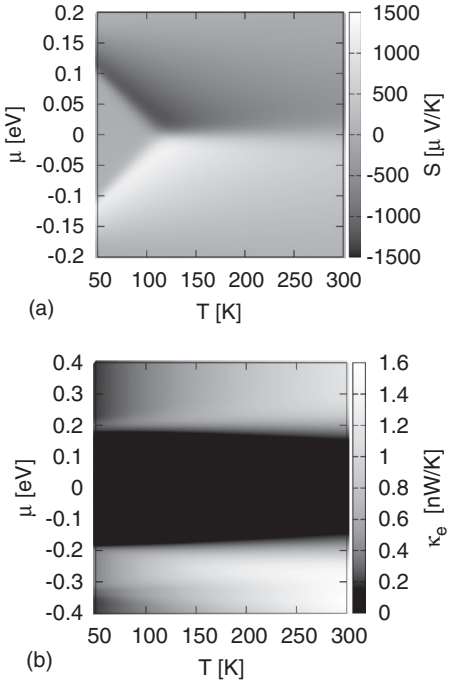

FIG. 3. Thermopower S (a) and electronic thermal conductance κ_e (b) of zSiNRs in the AFM configuration as a function of the chemical potential μ and temperature, calculated for $N = 5$ within the GGA approximation.

energy gap, let us analyze magnitude of S in the gap for different temperatures, as shown in Fig. 2(a). It is evident that the maxima of $|S|$ move towards the gap edges with decreasing T, and S almost vanishes then in a wide region of μ between the two peaks in $|S|$. The plateaus of zero S become broader with decreasing T. A rough estimate shows that the maximum is roughly at a distance of an order of several kT (about 10 kT) from the corresponding gap edge. This relatively large distance follows from two facts: (i) long tail of the Fermi-Dirac distribution function, and (ii) different temperature dependence of the functions L_1 and L_0 which determine S. Due to the factor $E - \mu$ in L_1, this function decreases with decreasing temperature faster than L_0 does. Since $S \sim L_1/L_0$, the interplay of the T dependence of both functions leads to the maxima of $|S|$ as well as to vanishing S well inside the gap for low T. This behavior is even more evident in Fig. 3(a), where S for μ in the gap is presented in a grayscale as a function of μ and T. It is evident that at low temperatures position of the maximum of $|S|$ departs from the gap edges almost linearly with increasing T. This linear variation stops at a specific temperature [$\sim$100 K in Fig. 3(a)], at which the maximum appears close to the gap center. Then, the maximum becomes weaker and slightly departs from the gap center with a further increase in T. For T lower than 100 K, there is a wide region [of triangle shape, clearly visible in Fig. 3(a)], where the thermopower S vanishes. Above 100 K, S vanishes only in the gap center, as already discussed above.

In Fig. 2(c), the thermal conductance due to electron transport κ_e is presented as a function of μ. This figure clearly shows that the conductance κ_e is strongly suppressed for μ in the energy gap. However, it significantly increases when the chemical potential is outside the gap (in the regions of

nonzero transmission), even at low temperatures. The range of μ, where κ_e is considerably suppressed, depends on the nanoribbon width and also weakly on temperature [see the inset in Fig. 2(c)]. It is interesting to note that for higher temperatures, a small maximum develops in the vicinity of $\mu = 0$. Such a maximum also appears in other systems.[25] The T dependence of κ is shown explicitly in Fig. 3(b), where κ is presented as a function of μ and T. Indeed, one can note the maximum developing at $\mu = 0$ for higher temperatures.

B. FM configuration

Now, let us consider the FM configuration. Although energy of this configuration is slightly higher than that of the AFM state, it can be stabilized by an external magnetic field. From Fig. 1(d) follows that there is no energy gap in the FM configuration, and the system behaves like a metal with a constant transmission function in a certain region of chemical potentials close to $\mu = 0$. Below that region (negative μ), there is a wide maximum in transmission for majority spins (spin $\uparrow$), whereas above (positive μ) a narrow peak in transmission appears for minority spins (spin $\downarrow$). Apart from this, transmission only weakly depends on the nanoribbon width. Numerical results on the transport parameters in the FM state are presented in Fig. 4. The electrical conductance G and the thermal conductance κ_e, calculated for several temperatures, are shown in Figs. 4(a) and 4(b), respectively. Both G and κ_e are constant for small values of μ, and display maxima for relatively high p- and n-type doping, which follow from the maxima in transmission function for majority and minority spins, respectively. In Fig. 5, the T dependence of G is shown explicitly as a function of μ and T. Variation of the conductance G with temperature is rather weak, as is also evident form Fig. 4(a).

Due to the gap existing in the AFM state and its absence in the FM state, electrical and heat transport are significantly different in these two configurations. More specifically, the conductance G and heat conductance κ_e at low doping are considerably larger in the FM state. Thus, one can observe a large magnetoresistance (MR) defined quantitatively as $\mathrm{MR} = (G_{\mathrm{FM}} - G_{\mathrm{AFM}})/(G_{\mathrm{FM}} + G_{\mathrm{AFM}})$, where G_{AFM} and G_{FM} are the total electrical conductances in the AFM and FM states, respectively. The magnetoresistance of nanoribbons corresponding to $N = 5$ is presented in Fig. 6 as a function of the chemical potential. For small p- and n-type dopings, MR achieves values practically equal to 1 since G_{AFM} is close to zero due to the energy gap. For higher doping, a negative magnetoresistance can be observed. These results clearly show that narrow zSiNRs can be important elements for spintronic devices, in which magnetic configuration can be easily changed from the AFM to FM states by an external magnetic field.

The thermopower S in the FM configuration, calculated for several values of temperature, is presented in Fig. 4(c). When the chemical potential is changed, S displays several peaks with intensities weakly dependent on temperature. These peaks are now remarkably smaller than in the AFM configuration. In particular, there is a region of small values of μ, where S is practically suppressed to zero at low temperatures, which is a consequence of a constant transmission in the FM

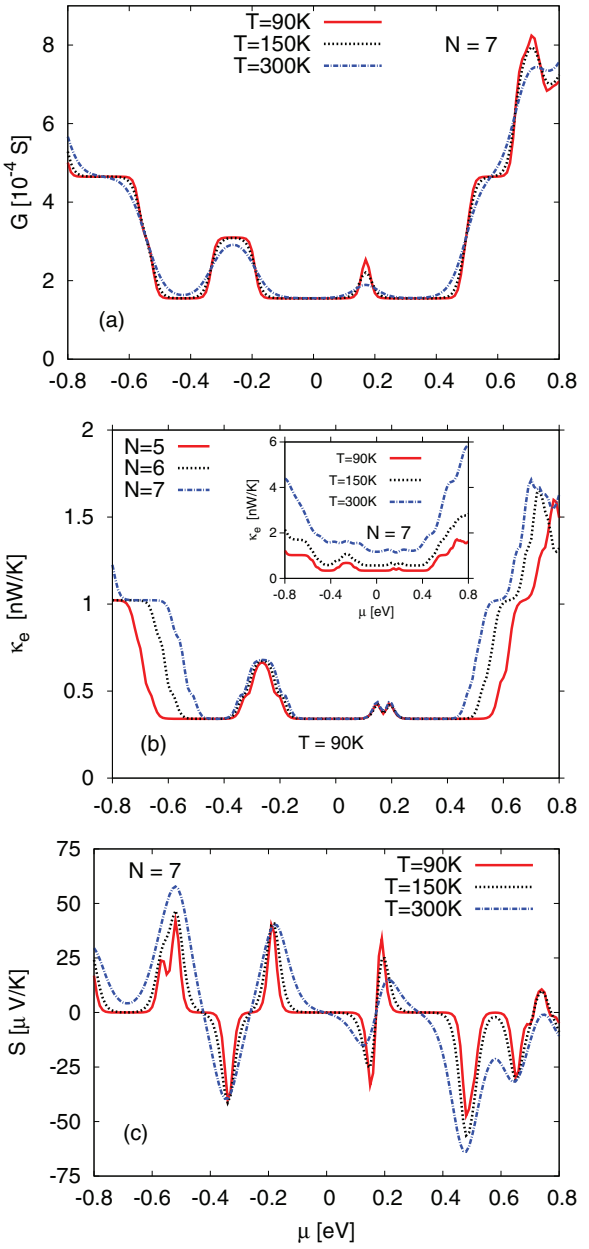

FIG. 4. (Color online) Electric conductance G (a), electronic thermal conductance κ_e (b), and thermopower S (c) in the FM state, calculated as a function of chemical potential within GGA for given values of N and T.

configuration close to the Dirac points. This region becomes narrower with increasing temperature, but S is still very small. Comparing the results presented in Figs. 2(a) and 4(c), one can conclude that the thermopower remarkably changes with magnetic configuration. To describe this dependence, one can introduce the magnetothermopower (MTP), defined quantitatively as $\mathrm{MTP} = (S_{\mathrm{FM}} - S_{\mathrm{AFM}})/(|S_{\mathrm{FM}}| + |S_{\mathrm{AFM}}|)$. Such a definition is convenient as it allows avoiding artifacts in the regions, where the thermopowers in both configurations have opposite signs and are similar in magnitude. The calculated MTP, presented in Fig. 6(b), is close to ± 1 in wide regions of μ in the vicinity of $\mu = 0$. This is because the thermopower in the FM configuration is then negligibly small in comparison

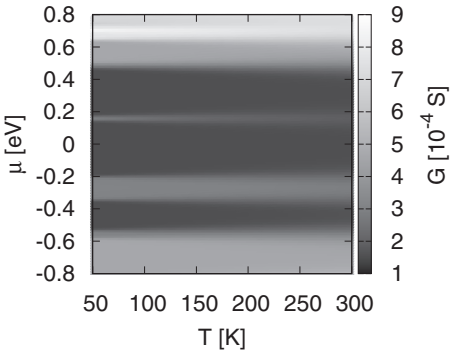

FIG. 5. Electric conductance G in the FM state as a function of chemical potential μ and temperature T calculated within GGA for $N = 7$.

to that in the AFM configuration. Thus, varying magnetic configuration one can easily change not only electrical resistance of the system, but also the voltage generated by a temperature gradient.

C. AP configuration

By applying a specific magnetic field, one can force the antiparallel (AP) configuration, in which the spin polarization in the left part of the nanoribbon is opposite to that in the right part. Thus, the AP state corresponds to the situation

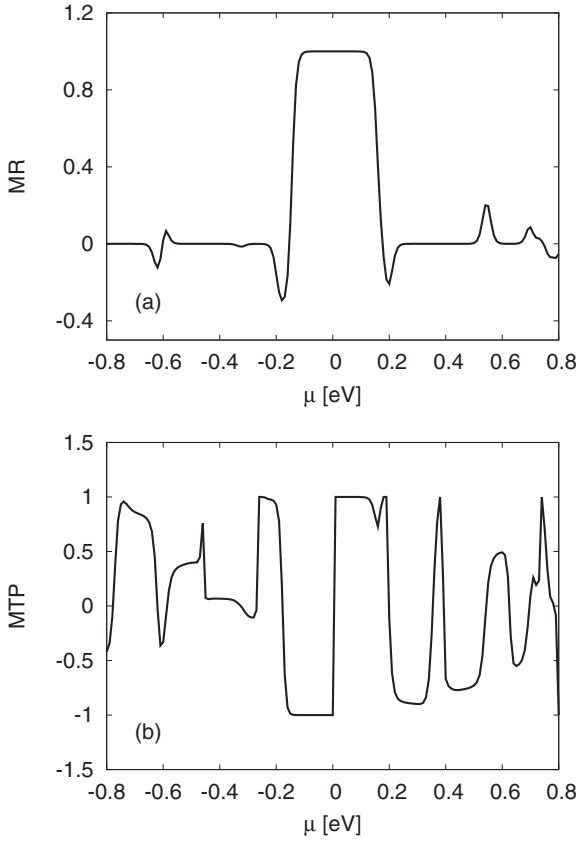

FIG. 6. Magnetoresistance MR (a) and magnetothermopower MTP (b) associated with a change from the AFM to FM states as a function of μ, calculated within the GGA approximation for $N = 5$ and $T = 90$ K.

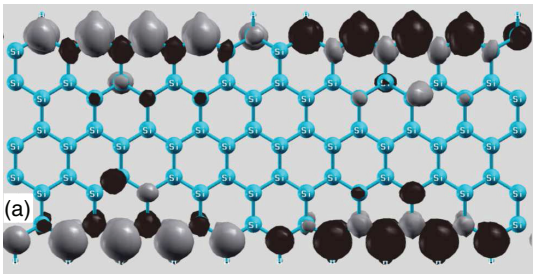

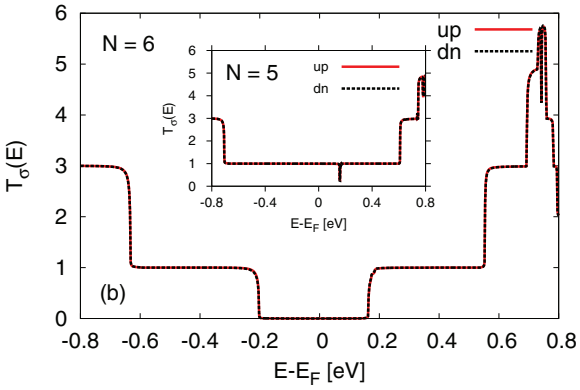

FIG. 7. (Color online) Spin density (a) and transmission $T_\sigma(E)$ for $N = 6$ (b) in the AP configuration. The inset in (b) shows the transmission for $N = 5$. Results obtained within the GGA approximation.

when the left and right electrodes are polarized antiparallel, as presented in Fig. 7(a). Electronic transport in such a configuration strongly depends on the ribbon widths. For N odd, $N = 5,7$, there is no gap in the band structure and the transmission is finite and constant in the vicinity of $\mu = 0$, while for $N = 6$ a gap opens near $\mu = 0$ [see Fig. 7(b)]. Note the band structure and transmission are now independent of spin orientation.[10] Thus, transport is strongly suppressed in the nanoribbons with $N = 6$, and the corresponding electrical and thermal conductances are small as compared to those for $N = 5,7$. This is shown in Fig. 8(a), where the thermal conductance is presented for nanoribbons of different widths and at different temperatures. Note the vanishingly small conductance in the region close to $\mu = 0$ for nanoribbons with $N = 6$, and no such suppression for other ribbons. Due to the gap existing for $N = 6$, there is a large change in the electric and heat conductances when magnetic configuration is changed from the AP to FM state. A large magnetoresistance appears especially for chemical potentials close to $\mu = 0$ [see Fig. 8(b)]. Much lower MR is expected for for nanoribbons with odd N.

The thermopower in the AP configuration also strongly depends on the ribbon width. Due to the presence of the energy gap for $N = 6$, it is considerably enhanced in the vicinity of small μ, similarly as in the case of AFM state [see Fig. 8(c)]. Accordingly, for ribbons with $N = 6$, a large MTP effect can be observed when the configuration is changed from the AP state to the FM one [see Fig. 8(d)]. Absolute value of MTP is close to unity in a wide range of chemical potential around $\mu = 0$. On the other hand, for zSiNRs with $N = 5$ and 7, the thermopower S in the AP configuration is rather small in the

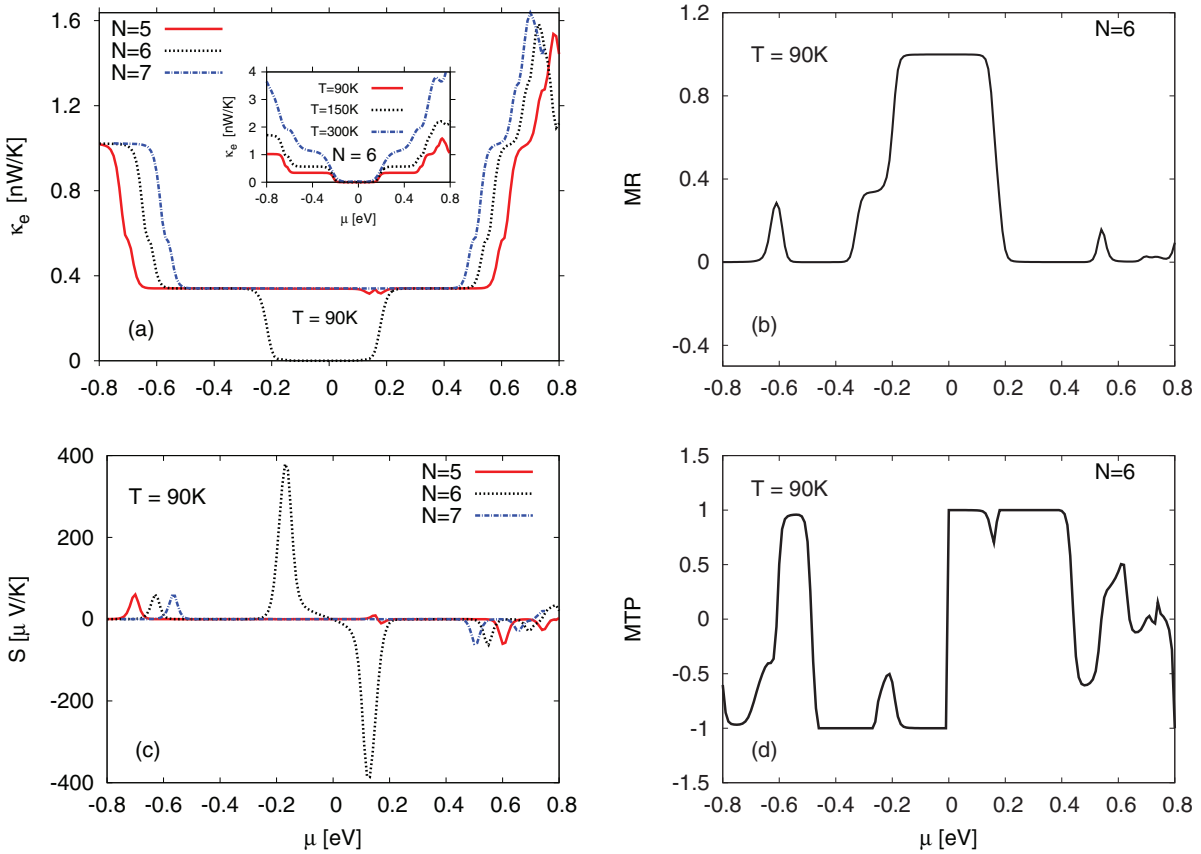

FIG. 8. (Color online) Electronic thermal conductance (a) and thermopower (c) as a function of μ for the AP configuration, calculated within the GGA approximation. Parts (b) and (d) present MR and MTP associated with transition from AP to FM configurations.

vicinity of $\mu = 0$. All this demonstrates a large influence of the ribbon width on transport properties and thermopower in the AP configuration, whereas the ribbon width has only a weak influence on transport in the AFM and FM configurations.

D. Comparison of the GGA and LDA methods

The results of *ab initio* calculations presented in the previous sections were based on the GGA method. These results clearly show that the energy gap, which appears in the AFM and AP configurations, has a strong influence on the transport and thermoelectric coefficients (see Figs. 2 and 8). It is also well known that accurate determination of the energy gap is the main problem in the DFT procedures, and the width of the gap can depend on the used approximations. Therefore, it seems reasonable to compare the results achieved within two main *ab initio* approximations, namely, GGA and LDA. Here, we limit considerations to the AFM case since the main conclusions also apply to the AP configuration with an energy gap. On the other hand, the results for configurations with constant and nonzero transmission in the vicinity of Fermi energy, namely, for the FM state and AP configuration with $N = 5,7$, only weakly depend on the used approximation.

In Fig. 9, we compare the results obtained for the AFM configuration within GGA and LDA methods. As a general rule, the energy gap calculated with the use of LDA is remarkably narrower than for GGA. This, in turn, has a considerable influence on the transmission function, leading to different behavior of the electrical and thermal transport. Accordingly, at low temperatures, the electrical conductance G and thermal conductance κ_e, calculated within LDA method, are suppressed in a narrower range of chemical potentials [see Figs. 9(a) and 9(b)]. These changes are even more pronounced at higher temperatures, where κ_e(LDA) strongly increases revealing a quite remarkable peak in the vicinity of small μ. Results obtained for the thermopower S also depend on the calculation scheme. This is because the thermopower S strongly depends on the gap width. From Fig. 9(c) follows that the dominant peaks in S are suppressed and also shifted to the region of smaller μ for the LDA method. There is also some asymmetry in the peak intensities for negative and positive μ. The results calculated within the LDA approximation for higher temperatures are consistent with those presented by Pan *et al.*[15] The strong asymmetry obtained in this reference is mainly due to the applied approximations. In Fig. 9(d), we show the thermoelectric efficiency $ZT_e = \frac{S^2GT}{\kappa_e}$. In this formula, the thermal conductance includes only electronic contribution. The calculated ZT_e is relatively high, mainly due to the strong suppression of electronic thermal conductance. The influence of phonon contribution to the thermal conductance will be discussed in Sec. V. One can also see that the thermoelectric efficiency is strongly dependent on the approach and for GGA it is much higher than for LDA. Moreover, since the gap is narrower in the LDA approximation, the corresponding peaks in ZT_e(LDA) are much closer to each other.

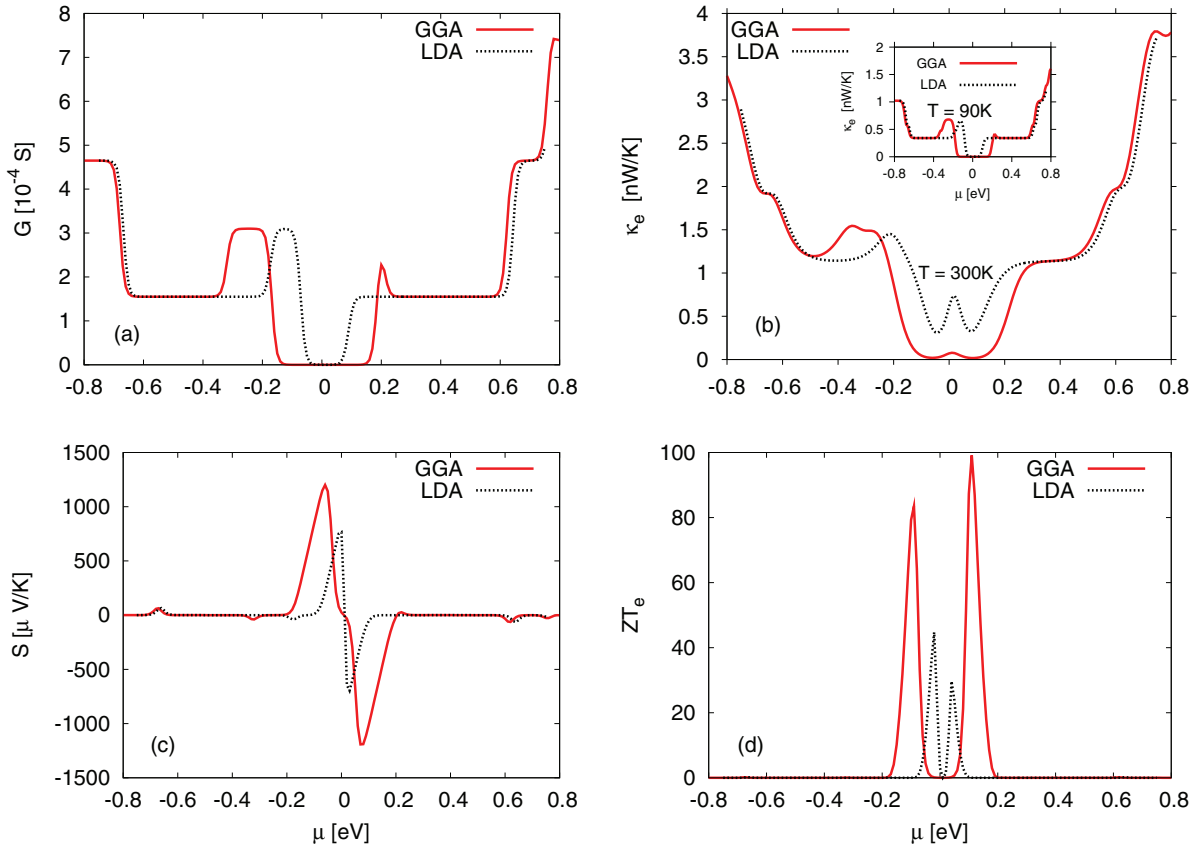

FIG. 9. (Color online) Electrical conductance G (a), electronic contribution to the thermal conductance κ_e (b), thermopower S (c), and figure of merit ZT_e (d) as a function of chemical potential, calculated for the AFM configuration within the GGA (solid lines) and LDA (dashed lines) approaches for $N = 5$ and $T = 90$ K.

IV. SPIN THERMOELECTRIC EFFECTS

When the two spin channels are not mixed by spin-flip transitions and can be treated as independent in the whole system, the temperature gradient can lead not only to charge accumulation at the ends of an open system, but also to spin accumulation. In other words, the temperature gradient gives rise not only to electrical voltage, but also to spin voltage. To observe the spin voltage, the length of the sample should be smaller than the spin-flip length. In the case under consideration, the system consists of a nanoribbon of length that is small enough, so the spin-flip scattering processes can be neglected. In fact, the system is a part of a long nanoribbon, whose outer parts form two external leads (electrodes). Thus, spin thermoelectric properties can be observed, and we will focus especially on the spin Seebeck effect. Moreover, the spin accumulation leads not only to the spin Seebeck effect, but also modifies the conventional electrical thermopower (Seebeck effect) as well as the electronic term in the heat conductance.

When the two spin channels are independent, one can introduce spin-dependent thermopower S_σ ($\sigma = \uparrow, \downarrow$), defined as $S_\sigma = -\frac{\Delta V_\sigma}{\Delta T} = -\frac{L_{1\sigma}}{|e|TL_{0\sigma}}$. The spin-dependent thermopower corresponds to a spin-dependent voltage generated by a temperature gradient.[25] The spin-dependent moments $L_{n\sigma}$, which appear in the above expression, are calculated with spin-dependent transmission functions $T_\sigma(E)$. Generally, one can define then charge thermopower $S_c = \frac{1}{2}(S_\uparrow + S_\downarrow)$ as well as spin thermopower $S_s = \frac{1}{2}(S_\uparrow - S_\downarrow)$. Both S_c and S_s, calculated for the FM state at low temperature, are presented in Fig. 10 as a function of μ. Due to constant transmission in the FM configuration, S_c and S_s are practically equal to zero in a wide range of small μ. For higher values of μ, both S_c and S_s show several peaks. It is interesting to note that intensities of the corresponding peaks in S_c and S_s are similar. In systems with p-type doping, and in the vicinity of chemical potential close to -0.2 eV, charge and spin thermopowers are

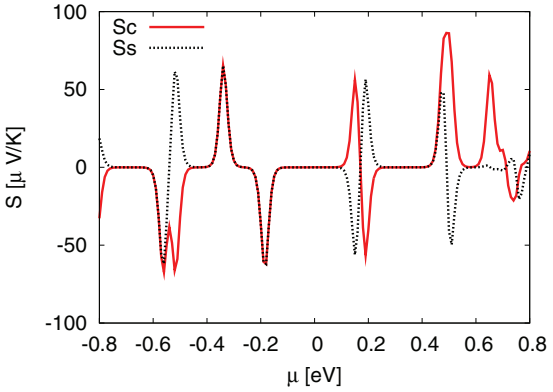

FIG. 10. (Color online) Charge (solid line) and spin (dashed line) thermopower as a function of chemical potential calculated for the FM configuration within GGA for $N = 7$ and $T = 90$ K.

practically equal and change with μ in a similar way. On the other hand, for n-type doping in the vicinity of $\mu \approx 0.2$ eV, they have similar values but opposite signs. Such a behavior is a result of the strong dependence of the transmission function on spin orientation. More specifically, transmission for majority spins shows a broad maximum for negative values of energy, whereas it is constant for minority spins. Therefore, in this region practically there is no contribution to S_c and S_s from minority spins and both quantities behave in a similar way. On the other hand, for positive μ the main contribution comes from minority spins, which results in opposite signs of S_c and S_s. The charge thermopower in spin-polarized systems is usually higher than the spin thermopower. It seems that the very peculiar behavior of thermopower in zSiNRs is a unique feature of the system under consideration.

V. THERMAL CONDUCTANCE DUE TO PHONONS

The transport coefficients calculated above were limited to electronic contributions only. However, an important contribution to heat current comes from phonons. In some specific situations, especially when charge current is strongly suppressed, e.g., in the energy gap, this contribution to heat current may be dominant. This, in turn, can have a significant impact on thermoelectric efficiency, which may be remarkably reduced as well. In this section, we present numerical results on the role of phonon term in the heat conductance in silicene. We will use two different methods to calculate the phonon dispersions: *ab initio* and the model known as 4 nearest-neighbor force constants (4NNFC). Parameters of the latter model will be determined from fitting of the corresponding phonon spectrum to the one from *ab initio* calculations.

A. Force constants for silicene in the 4NNFC model

The 4NNFC model, describing the dynamical matrix by 12 parameters in the fourth-neighbor approximation, was introduced by Saito[39] for carbon nanotubes, and subsequently applied to graphene.[40] Three force constant parameters are introduced for a given atom and its neighbor: ϕ_r for radial displacement (bond stretching), ϕ_{ti} for in-plane tangential displacement, and ϕ_{to} for out-of-plane displacement. When the direction from a given atom to its neighbor coincides with the x axis, the resultant force-constant tensor K is diagonal:

$$K = \begin{pmatrix} \phi_r & 0 & 0 \\ 0 & \phi_{ti} & 0 \\ 0 & 0 & \phi_{to} \end{pmatrix}. \tag{4}$$

In a general case, when the direction from a given atom to its neighbor is described by spherical angles ϕ and θ, one has to rotate the force-constant tensor by the following orthogonal transformation: $K' = R_x(\theta)^\dagger\, R_z(\phi)^\dagger\, K\, R_z(\phi)\, R_x(\theta)$, where $R_z(\phi)$ is the matrix of rotation around the z axis by ϕ, and $R_x(\theta)$ is the matrix of rotation around the x axis by θ.

We varied the 12 force-constant parameters to obtain the best fit to *ab initio* calculations. Since the structure of buckled silicene is not flat, the dynamical matrix is not invariant under infinitesimal in-plane rotations. Therefore, we do not apply the rotational invariance condition for in-plane and out-of plane tangential force constants $\phi_t^{(1)} + 6\phi_t^{(2)} + 4\phi_t^{(3)} + 14\phi_t^{(4)} = 0$, which is valid for graphene.[40] The *ab initio* calculations were performed in 50 k points along the high-symmetry path in the first Brillouin zone of hexagonal two-dimensional lattice with the use of ABINIT code.[41] For calculation of the phonon spectra, the code relies on the density-functional perturbation theory.[42] The force-constants parameters were varied to minimize the sum of squares of deviations from *ab initio* values of the phonon frequencies. Table I presents the obtained force constants, which correspond to the global minimum.

TABLE I. Force-constants for silicene in the 4NNFC model.

Neighbor	ϕ_r	ϕ_{ti}	ϕ_{to}
1st	2.0639	15.9965	0.3814
2nd	−0.8961	0.9010	0.0683
3rd	0.2537	−0.9737	0.1396
4th	0.3005	−0.1067	−0.1006

Figure 11 presents the comparison of phonon dispersion relations calculated within the 4NNFC model with the corresponding *ab initio* results. In turn, Table II contains comparison of the phonon frequencies at high-symmetry points from *ab initio* calculations with those obtained by the 4NNFC model. There are some quantitative differences, but qualitative agreement is satisfactory.

B. Phonon conductance for silicene nanoribbons

Next, the obtained force constants are used to determine the phonon dispersion relations for zigzag silicene nanoribbons within the 4NNFC model. From these dispersion relations one can determine the phonon transmission function $T(\omega)$, which is equal to the number of bands at the phonon energy ω.

Phonon contribution to the heat conductance κ_{ph} can be determined by integration of the transmission function, according to the following formula:

$$\kappa_{ph} = \frac{1}{2\pi} \int_0^\infty \hbar\omega\, T(\omega)\, \frac{\partial n}{\partial T}\, d\omega, \tag{5}$$

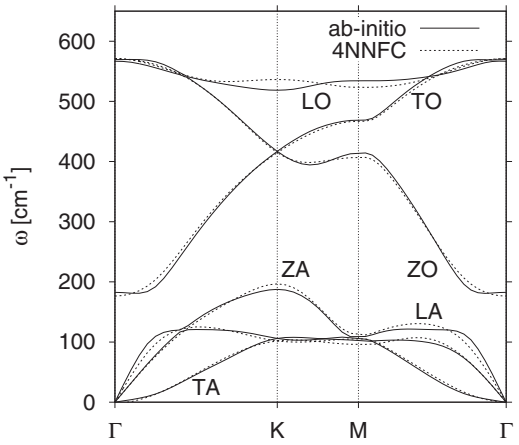

FIG. 11. Phonon dispersion relation for planar silicene. Phonon modes denoted as in Ref. 43.

TABLE II. Phonon frequencies in cm^{-1} at high-symmetry points.

Point	Mode	*Ab initio*	4NNFC
Γ	ZO	183	176
	TO/LO	568	571
K	TA/LA	106	102
	ZA	187	188
	TO/ZO	417	415
	LO	519	536
M	TA	102	96
	ZA	105	105
	LA	110	112
	ZO	414	407
	TO	469	467
	LO	534	523

where n is the Bose-Einstein distribution function of equilibrium phonons at temperature T. The phonon contribution to heat conductance for zSiNRs with $N = 4$ is presented in Fig. 12 as a function of temperature. The inset to Fig. 12 shows the dependence of the phonon conductance within the 4NNFC model on the width of zSiNRs (the points correspond to $N = 4,5,6,7,8$). As expected, κ_{ph} depends linearly on the nanoribbon width. This phonon term in heat conductance is compared there with that obtained from the *ab initio* method. The *ab initio* transmission function was obtained from phonon spectrum calculated with use of phonopy code,[44] which realizes the Parlinski-Li-Kawazoe method, based on the supercell approach with the finite displacement method.[45] Forces acting on atoms with respect to their displacements, needed by this method, were calculated with the VASP code[46,47] using PAW pseudopotentials.[48] We used the VASP code as it turned out to be reliable and less time consuming. The results obtained within the VASP code and 4NNFC model are comparable: the difference is minor at low temperatures, but grows as the temperature increases.

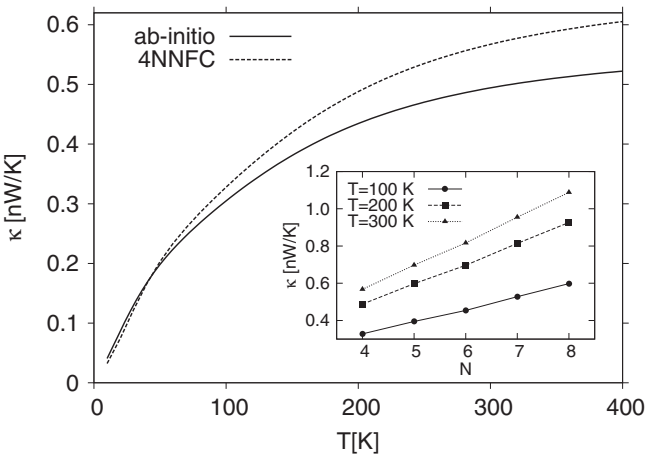

FIG. 12. Phonon contribution to heat conductance of zSiNRs corresponding to $N = 4$ as a function of temperature, calculated within the 4NNFC and *ab initio* models. The inset shows the phonon contribution to heat conductance calculated with the 4NNFC model as a function of N (zSiNRs width).

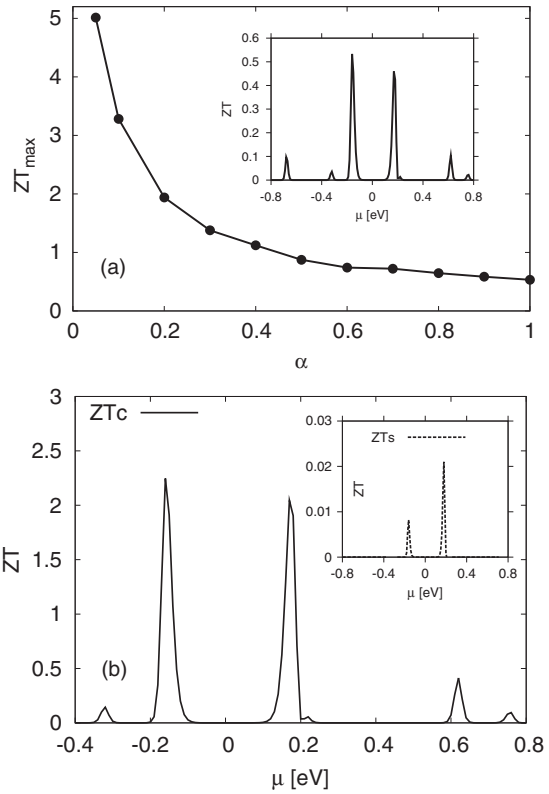

FIG. 13. (a) Maximum of ZT for AFM state as a function of scaling parameter α. The inset shows ZT as a function of chemical potential. (b) ZT_c and ZT_s (inset) for the FM configuration. The results are for $T = 90$ K, $N = 5$, and within GGA approach.

C. Influence of phonons on thermoelectrical efficiency

The influence of phonons on thermoelectric efficiency ZT is presented in Fig. 13(a) for the AFM case (inset). The calculated phonon conductance strongly suppresses ZT, which appears to be lower than 1 in the whole region under consideration. We note that the authors of Ref. 15, using molecular dynamic simulations, obtained relatively low phonon conductance, even at high temperatures. This shows that the accurate determination of κ_{ph} in silicene nanoribbons is a difficult task. Moreover, the interaction between the narrow nanoribbons and a substrate as well as electron-phonon coupling can be important and may influence the phonon conductance. One can expect that interaction with a substrate will considerably reduce κ_{ph}. To take into account the reduction of thermal conductance due to a substrate, as well as some differences in estimation of the phonon conductance when using different calculation methods, we scale κ_{ph} with a parameter α, similarly as in Ref. 49, namely, κ_{ph} determined in the previous section is expressed in the form $\alpha\kappa_{ph}$ and we discuss the influence of the parameter α on the maximum value of ZT. According to Fig. 13(a), one can see that α strongly affects the efficiency. The main maximum in ZT is considerably suppressed even for $\alpha = 0.05$. For higher values of α, the changes are not so rapid, but ZT becomes relatively low.

It is interesting that relatively high efficiency $ZT_c = S_c^2(G_\uparrow + G_\downarrow)T/[(\kappa_{e\uparrow} + \kappa_{e\downarrow}) + \kappa_{ph}]$ can be obtained for FM configuration when the two spin channels are not mixed

and spin effects are important. As presented in Fig. 13(b), maximum efficiency is as high as 2.5 despite considerable phonon conductance. On the other hand, the spin part $ZT_s = S_s^2(G_\uparrow - G_\downarrow)T/[(\kappa_{e\uparrow} + \kappa_{e\downarrow}) + \kappa_{ph}]$ is considerably suppressed.

VI. SUMMARY AND CONCLUSIONS

We have carried out detailed analysis of linear thermoelectric effects in silicene zigzag nanoribbons. Such nanoribbons may reveal several stable magnetic configurations of the edge magnetic moments: AFM (magnetic moments at one edge are opposite to those at the other edge), FM (magnetic moments at the two edges are align in parallel), and AP (magnetic moments in left part of the nanoribbon are opposite to those in the right part). The former configuration (AFM) is of the lowest energy, but the other two can be stabilized by an external magnetic field. Transmission function reveals a relatively wide gap at the Fermi level in the case of the AFM state, while no gap appears in the FM state.

Thermoelectric parameters have been calculated in two limiting situations: (i) no spin accumulation can build up in the leads, and (ii) spin accumulation can appear due to slow or absence of spin relaxation. In the latter case, spin thermoelectric effects can occur, especially the spin thermopower, which effectively describes spin voltage generated by a temperature gradient. Electronic contributions to the thermoelectric effects reflect the presence of the gap, where the thermopower is significantly enhanced. We have also calculated the phonon contribution to heat conductance, and thus also to the thermoelectric efficiency. The phonon term in the heat conductance is dominant when the Fermi level is inside the energy gap, while both electronic and phonon contributions are comparable for Fermi level outside the gap. Thus, the phonon contribution suppresses the high value of the thermoelectric efficiency as well as of the spin thermoelectric efficiency, which were obtained for the Fermi levels inside the energy gap and when only the electronic term in the heat conductance was taken into account.

For calculating the electronic and phonon transmission functions, we used various numerical procedures and approximations. There are some quantitative differences in the results obtained with those methods, especially when the gap appears at the Fermi level of the nanoribbons. However, there is a good qualitative agreement between the results obtained with different methods.

We note that the results presented in this paper were obtained for pristine silicene nanoribbons, with well-defined zigzag edges. Similarly as in graphene, one can expect that edge roughness, impurities, and defects can influence transport and thermoelectric properties. Recent studies of thermal conductance of GNRs indicate that edge roughness considerably suppresses the lattice component κ_{ph}.[50–53] The edge disorder can also strongly reduce the phonon transport in zGNRs, but only weakly influences electronic contribution to κ. However, the electron transmission $T(E)$ is modified, mainly in the vicinity of Dirac points.[54–56] The width of the gap depends on the disorder due to edge states leading to localized levels. Generally, all the modifications can enhance thermoelectric figure of merit in GNRs.[54] Very recently, the interplay between bulk and edge states induced by the Rashba spin-orbit coupling in zSiNRs has been investigated in the presence of an external electric field.[57] It has been shown that the states with opposite velocities can open spin-dependent subgaps which influence spin-polarized current. Our preliminary *ab initio* calculations performed for zSiNRs with impurity atom (Al, P) at one of the ribbon edges reveal modifications of the transmission function $T(E)$. In the FM, state they lead to enhancement of spin and charge thermopower. This problem will be considered in a forthcoming paper.

ACKNOWLEDGMENTS

This work was supported by the National Science Center in Poland as the Project No. DEC-2012/04/A/ST3/00372. Numerical calculations were performed at the Interdisciplinary Centre for Mathematical and Computational Modelling (ICM) at Warsaw University and partly at SPINLAB computing facility at Adam Mickiewicz University.

[1] B. Dlubak, M.-B. Martin, C. Deranlot, B. Servet, S. Xavier, R. Mattana, M. Sprinkle, C. Berger, W. A. DeHeer, F. Petroff, A. Anane, P. Seneor, and A. Fert, Nat. Phys. **8**, 557 (2012).

[2] K. S. Novoselov, A. K. Geim, S. V. Morozov, D. Jiang, M. I. Katsnelson, I. V. Grigorieva, S. V. Dubonos, and A. A. Firsov, Nature (London) **438**, 197 (2005).

[3] C. Berger, Z. Song, X. Li, X. Wu, N. Brown, C. Naud, D. Mayou, T. Li, J. Hass, A. N. Marchenkov, E. H. Conrad, P. N. First, and W. A. de Heer, Science **312**, 1191 (2006).

[4] B. Aufray, A. Kara, S. Vizzini, H. Oughaddou, C. Léandri, B. Ealet, and G. Le Lay, Appl. Phys. Lett. **96**, 183102 (2010).

[5] P. D. Padova, C. Quaresima, B. Olivieri, P. Perfetti, and G. Le. Lay, Appl. Phys. Lett. **98**, 081909 (2011).

[6] P. Vogt, P. De Padova, C. Quaresima, J. Avila, E. Frantzeskakis, M. C. Asensio, A. Resta, B. Ealet, and G. Le Lay, Phys. Rev. Lett. **108**, 155501 (2012).

[7] A. Kara, H. Enriquez, A. P. Seitsonen, L. C. Lew, Yan Voon, S. Vizzini, B. Aufray, and H. Oughaddou, Surf. Sci. Rep. **67**, 1 (2012).

[8] M. Ezawa, New J. Phys. **14**, 033003 (2012); J. Phys. Soc. Jpn. **81**, 064705 (2012).

[9] A. Dyrdal and J. Barnas, Phys. Status Solidi RRL **6**, 340 (2012).

[10] C.-C. Liu, H. Jiang, and Y. Yao, Phys. Rev. B **84**, 195430 (2011).

[11] S. Cahangirov, M. Topsakal, and S. Ciraci, Phys. Rev. B **81**, 195120 (2010); M. Miller and F. J. Owens, Chem. Phys. **381**, 1 (2011); Y.-L. Song, Y. Zhang, J.-M. Zhang, D.-B. Lu, and K.-W. Xu, Physica B (Amsterdam) **406**, 69 (2011); Ch. Zhang and Sh. Yan, J. Phys. Chem. C **116**, 4163 (2012).

[12] O. V. Yazyev, Phys. Prog. Rep. **73**, 056501 (2010).

[13] Ch. Xu, G. Luo, Q. Liu, J. Zheng, Z. Zhang, S. Nagase, Z. Gao, and J. Lu, Nanoscale **4**, 3111 (2012).

[14]J. Kang, F. Wu, and J. Li, Appl. Phys. Lett. **100**, 233122 (2012).
[15]L. Pan, H. J. Liu, X. J. Tan, H. Y. Lv, J. Shi, X. F. Tang, and G. Zheng, Phys. Chem. Chem. Phys. **14**, 13588 (2012).
[16]W. Y. Kim and K. S. Kim, Nat. Nanotechnol. **3**, 408 (2008).
[17]F. Munoz-Rojas, J. Fernandez-Rossier, and J. J. Palacios, Phys. Rev. Lett. **102**, 136810 (2009).
[18]R. Venkatasubramanian, E. Siivola, T. Colpitts, and B. O'Quinn, Nature (London) **413**, 597 (2001).
[19]A. I. Hochbaum, R. Chen, R. D. Delgado, W. Liang, E. C. Garnett, M. Najarian, A. Majumdar, and P. Yang, Nature (London) **451**, 163 (2008).
[20]T. C. Harman, P. J. Taylor, M. P. Walsh, and B. E. LaForge, Science **297**, 2229 (2002).
[21]N. B. Duarte, G. D. Mahan, and S. Tadigadapa, Nano Lett. **9**, 617 (2009).
[22]M. Walter, J. Walowski, V. Zbarsky, M. Münzenberg, M. Schäfers, D. Ebke, G. Reiss, A. Thomas, P. Peretzki, M. Seibt, J. S. Moodera, M. Czerner, M. Bachmann, and Ch. Heiliger, Nat. Mater. **10**, 742 (2011).
[23]N. Liebing, S. Serrano-Guisan, K. Rott, G. Reiss, J. Langer, B. Ocker, and H. W. Schumacher, Phys. Rev. Lett. **107**, 177201 (2011).
[24]K. Uchida, S. Takahashi, K. Harii, J. Ieda, W. Koshibae, K. Ando, S. Maekawa, and E. Saitoh, Nature (London) **455**, 778 (2008).
[25]R. Świrkowicz, M. Wierzbicki, and J. Barnaś, Phys. Rev. B **80**, 195409 (2009).
[26]Y.-W. Son, M. L. Cohen, and S. G. Louie, Nature (London) **444**, 347 (2006).
[27]L. Pisani, J. A. Chan, B. Montanari, and N. M. Harrison, Phys. Rev. B **75**, 064418 (2007).
[28]F. Munoz-Rojas, J. Fernandez-Rossier, and J. J. Palacios, Phys. Rev. Lett. **102**, 136810 (2009).
[29]Y. Ding and J. Ni, Appl. Phys. Lett. **95**, 083115 (2009).
[30]M. Zeng, W. Huang, and G. Liang, Nanoscale **5**, 200 (2013).
[31]S. Cheng, J. Phys: Condens. Matter **24**, 385302 (2012).
[32]D. Sanchez-Portal, P. Ordejon, E. Artacho, and J. M. Soler, Int. J. Quantum Chem. **65**, 453 (1997).
[33]M. Brandbyge, J.-L. Mozos, P. Ordejon, J. Taylor, and K. Stokbro, Phys. Rev. B **65**, 165401 (2002).
[34]Y.-W. Son, M. L. Cohen, and S. G. Louie, Phys. Rev. Lett. **97**, 216803 (2006).
[35]D. M. Ceperley and B. J. Alder, Phys. Rev. Lett. **45**, 566 (1980).
[36]J. P. Perdew and A. Zunger, Phys. Rev. B **23**, 5048 (1981).
[37]J. P. Perdew, K. Burke, and M. Ernzerhof, Phys. Rev. Lett. **77**, 3865 (1996).
[38]C. D. Mahan, *Many-Particle Physics* (Plenum, New York, 2000).
[39]R. Saito, G. Dresselhaus, and M. S. Dresselhaus, *Physical Properties of Carbon Nanotubes* (Imperial College Press, London, 1998).
[40]J. Zimmermann, P. Pavone, and G. Cuniberti, Phys. Rev. B **78**, 045410 (2008).
[41]X. Gonze *et al*., Comput. Phys. Commun. **180**, 2582 (2009).
[42]X. Gonze, Phys. Rev. B **55**, 10337 (1997); X. Gonze and C. Lee, *ibid*. **55**, 10355 (1997).
[43]Y. C. Cheng, Z. Y. Zhu, and U. Schwingenschlögl, Europhys. Lett. **95**, 17005 (2011).
[44]A. Togo, F. Oba, and I. Tanaka, Phys. Rev. B **78**, 134106 (2008).
[45]K. Parlinski, Z. Q. Li, and Y. Kawazoe, Phys. Rev. Lett. **78**, 4063 (1997).
[46]G. Kresse and J. Hafner, Phys. Rev. B **47**, 558 (1993).
[47]G. Kresse and J. Furthmuller, Phys. Rev. B **54**, 11169 (1996).
[48]P. E. Blöchl, Phys. Rev. B **50**, 17953 (1994).
[49]T. Gunst, T. Markussen, A.-P. Jauho, and M. Brandbyge, Phys. Rev. B **84**, 155449 (2011).
[50]A. S. Nissimagoudar and N. S. Sankeshwar, Carbon **52**, 201 (2013).
[51]H. Karamitaheri, N. Neophytou, M. Pourfath, R. Faez, and H. Kosina, J. Appl. Phys. **111**, 054501 (2012).
[52]Z. Aksamija and I. Knezevic, Appl. Phys. Lett. **98**, 141919 (2011).
[53]W. Evans, L. Hu, and P. Klebinski, Appl. Phys. Lett. **96**, 203112 (2010).
[54]H. Sevincli and G. Cuniberti, Phys. Rev. B **81**, 113401 (2010).
[55]A. Cresti, N. Nemec, B. Biel, G. Niebler, F. Triozon, G. Cuniberti, and S. Roche, Nano Res. **1**, 361 (2008); E. R. Mucciolo, A. H. Castro Neto, and C. H. Lewenkopf, Phys. Rev. B **79**, 075407 (2009).
[56]D. A. Areshkin, D. Gunlycke, and C. T. White, Nano Lett. **7**, 204 (2007).
[57]Xing-Tao An, Yan-Yang Zhang, Jian-Jun Liu, and Shu-Shen Li, Appl. Phys. Lett. **102**, 213115 (2013).